Proceedings of the 2021 IEEE International
Conference on Intelligence and Safety for Robotics
Nagoya, Japan, March 4-6, 2021

Proposal of Fail-Safe Contact Motion Control and its Simulation using CRANE-X7

Hiroki Kito, Yoji Yamada, Jian Liu, Yasuhiro Akiyama and Shogo Okamoto

***Abstract*— Currently, human-robot collaboration has attracted remarkable interest among researchers. It is being considered for application in the field of manufacturing and an attention of a new risk regarding runaway motion on the robot side has been paid by our group. For example, if the robot runs away owing to a single fault, the robot and the worker may collide. Therefore, the runaway motions of robots need to be examined. We focus on not only a joint running away but also other active joints. If we can control them and reduce the amount of collision impact, a safe operation can be achieved at a fully secured level. Thus, we propose a fail-safe contact motion control and simulate its usefulness using CRANE-X7.**

I. Introduction

With the recent introduction of human-robot collaboration, there has been much debate on the new associated risks. The protective separation distance (PSD), which quantifies the minimum distance of separation for protection, [1] is defined as an international standard, and a considerable amount of research has been conducted on the practical application of speed separation monitoring (SSM), which is a requirement for the use of the PSD. There have been various studies on different topics [2] [3], including the introduction of SSM prototypes [4] safety and productivity evaluation of SSM [5], and implementation of SSM in a collaborative robot work cell [6]. Some studies have complemented PSD [7] [8], and some have examined avoidance behavior [9] [10] [10] Moreover, many researchers have debated about safety based on whether or not contact between robots and humans is allowed. Suita and Yamada et al. proposed the use of human somatic pain as a criterion for acceptability [11] [12] [13]. Other studies have proposed deformation tolerance limits [14], the correlation between pain and energy [15], and impact experiments using surrogate animal skin [16] [17]. In addition, according to the ISO 10218-1 standard [1] [18], the safety of workers must be ensured even in the event of a single failure in a safety-related system, and fault detection algorithms have been actively researched [19] [20] [21]. Here, we consider a case in which a single failure occurs in a robot. The worst case would be the maximization of one of the joint torques of the robot owing to a single failure. Yamada et al. [22] defined the space in which a robot can move in the event of a runaway situation up to the time of emergency stop as the potential runaway space of the workspace representation (PRAM-t). It was used to estimate the space in which the manipulator could move before stopping. Based on this, we extend the concept of PRAM-t and propose fail-safe contact motion control (FSCMC) as a safety strategy that may further improve the productivity of the system. The goal is to maintain human contact motion in a fail-safe manner at a fully secured level, which means that even in highly unlikely runaway conditions of manipulators, the risk of contact can be avoided. In this paper, the concept of FSCMC is proposed, and the practicality of FSCMC is evaluated by simulating a collision between a manipulator and a dummy skin.

All are with the Department of Mechanical Systems Engineering, Nagoya University, Nagoya, Japan.

II. Fail-safe contact motion control

In this chapter, we propose fail-safe contact motion control (FSCMC) as an attempt to reduce the risk of collision by using a sound joint when the joint of a manipulator runs out of control and contacts the human body.

A. Dynamics of manipulator

The dynamic properties of the manipulator are shown below.

$$\boldsymbol{M}(\boldsymbol{q})\ddot{\boldsymbol{q}} + \boldsymbol{C}(\boldsymbol{q}, \dot{\boldsymbol{q}}) + \boldsymbol{g}(\boldsymbol{q}) = \boldsymbol{\tau} - \boldsymbol{J}^T\boldsymbol{f} \tag{1}$$

where $\boldsymbol{q} \in \boldsymbol{R}^n$ is the vector of the joint angle, $\boldsymbol{M}(\boldsymbol{q})$ is the inertia matrix, $\boldsymbol{C}(\boldsymbol{q}, \dot{\boldsymbol{q}}) \in \boldsymbol{R}^n$ is the term for centrifugal and Coriolis forces, $\boldsymbol{g}(\boldsymbol{q}) \in \boldsymbol{R}^n$ is the term for gravity, and $\boldsymbol{f} \in \boldsymbol{R}^m$ is the external force applied to the end-effector. However, if $\boldsymbol{x} \in \boldsymbol{R}^n$ is the vector of the position of the end-effector, and $\boldsymbol{J}(\boldsymbol{q}) \in \boldsymbol{R}^{m\times n}$ is the Jacobian, the following equation is obtained:

$$\ddot{\boldsymbol{x}} = \boldsymbol{J}\boldsymbol{M}^{-1}(\boldsymbol{\tau} - \boldsymbol{C}(\boldsymbol{q}, \dot{\boldsymbol{q}}) - \boldsymbol{G}(\boldsymbol{q})) + \dot{\boldsymbol{J}}(\boldsymbol{q})\dot{\boldsymbol{q}} - \boldsymbol{J}\boldsymbol{M}^{-1}\boldsymbol{J}^T\boldsymbol{f} \tag{2}$$

The human body is then divided into a five-element matrix with viscoelastic parameters, as shown in Fig. 3. Considering the Maxwell model and defining the parametersk_1, k_2, k_3, c_2, c_3, displacement x_h, x_{h2}, x_{h3} and force f_r, we obtain the following three equations:

$$\begin{cases} f_r = k_1 x_h + k_2 x_{2h} + k_3 x_{3h} \\ k_2 x_{2h} = c_2(\dot{x}_h - \dot{x}_{2h}) \\ k_3 x_{3h} = c_3(\dot{x}_h - \dot{x}_{3h}) \end{cases} \tag{3}$$

Let the unit for indicating the direction of danger be the vector $\boldsymbol{h} \in \boldsymbol{R}^3$, and $\boldsymbol{f}$ be represented by

$$\boldsymbol{f} = f_r\boldsymbol{h}. \tag{4}$$

We define $\boldsymbol{u} \in \boldsymbol{R}^3$ as follows:

978-0-7381-4674-4/21/$31.00 ©2021 IEEE

$$\boldsymbol{u} = \boldsymbol{JM}^{-1}(\boldsymbol{\tau} - \boldsymbol{C}(\boldsymbol{q}, \dot{\boldsymbol{q}}) - \boldsymbol{G}(\boldsymbol{q})) + \dot{\boldsymbol{J}}(\boldsymbol{q})\dot{\boldsymbol{q}} \quad (5)$$

And Eq. 2 becomes like following;

$$\ddot{\boldsymbol{x}} = -\boldsymbol{JM}^{-1}\boldsymbol{J}^T\boldsymbol{u}_h fr + \boldsymbol{u} \quad (6)$$

Taking the inner product of both sides of the above equation and $\boldsymbol{h}$, and substituting f_r, the following equation is obtained:

$$\ddot{x}_h = -M_h(k_1 x + k_2 x_{2h} + k_3 x_{3h}) + u_h \quad (7)$$

With $\ddot{x}_h = \boldsymbol{h}^T\ddot{\boldsymbol{x}}$, $M_h = \boldsymbol{h}^T\boldsymbol{JM}^{-1}\boldsymbol{J}^T\boldsymbol{h}$, $u_h = \boldsymbol{h}^T\boldsymbol{u}$, let the Laplace-transformed x_h, x_{2h}, x_{3h}, and u_h be X_h, X_{2h}, X_{3h}, and U_h, respectively. By Laplace-transforming the equations and eliminatingX_{2h} and X_{3h}, we obtain

$$s^2 X_h = -M_h(k_1 + \frac{sk_2c_2}{k_2 + sc_2} + \frac{sk_3c_3}{k_3 + sc_3})X_h + U_h \quad (8)$$

Let U be the input and X_h be the output. Transfer function G is obtained for the system. Then, based on G, we obtain a state-space model with an input of u_h and an output of x_h.

B. Running away part

This section deals with the orbit calculation of the end-effector in the runaway part. As an example, consider the case in which the i-th joint generates a positive torque on the z-axis of rotation. Let's define the max torque of each joint as $\tau_{imax}\,(i = 1, ..., \mathrm{n})$. The torque vector where the i-th component is τ_{imax} and the other components are zero is $\boldsymbol{\tau}_{i+}$, and the torque vector where the i-th component is $-\tau_{imax}$ and the other components are zero is $\boldsymbol{\tau}_{i-}$. Then, the input is expressed as

$$\boldsymbol{u}_h = \boldsymbol{h}^T[\boldsymbol{JM}^{-1}(\boldsymbol{\tau}_{i+} - \boldsymbol{C}(\boldsymbol{q}, \dot{\boldsymbol{q}}) - \boldsymbol{G}(\boldsymbol{q})) + \dot{\boldsymbol{J}}(\boldsymbol{q})\dot{\boldsymbol{q}}] \quad (9)$$

By solving the aforementioned state-space model under initial conditions, we can obtain the trajectory of the end-effector.

C. Braking part

This section deals with the calculation of the trajectory of the end-effector in the brake part. As in the previous section, consider the case where the i-th joint generates a positive torque on the z-axis to the axis of rotation. Here, we define $\hat{\boldsymbol{\tau}}_j(j = 1, ..., n)$ as follows:

$$\begin{aligned} \text{If} \quad & \boldsymbol{h}^T \cdot \boldsymbol{JM}^{-1}\boldsymbol{\tau}_{j+} \leqq 0,\ \boldsymbol{\tau}_j = \boldsymbol{\tau}_{j+} \\ & \text{else} \quad \boldsymbol{tau}_j = \{\boldsymbol{\tau}_{j-} \end{aligned} \quad (10)$$

Then, we define the torque produced by the braking of the failed joint and the control of the healthy joint as follows:

$$\boldsymbol{\tau}_{ib} = (\sum_{j=1}^{n} \boldsymbol{\tau}_j) - \boldsymbol{\tau}_i + \boldsymbol{\tau}_{i-} \quad (11)$$

Then, the input can be defined as follows:

$$\boldsymbol{u}_h = \boldsymbol{h}^T[\boldsymbol{JM}^{-1}(\boldsymbol{\tau}_{ib} - \boldsymbol{C}(\boldsymbol{q}, \dot{\boldsymbol{q}}) - \boldsymbol{G}(\boldsymbol{q})) + \dot{\boldsymbol{J}}(\boldsymbol{q})\dot{\boldsymbol{q}}] \quad (12)$$

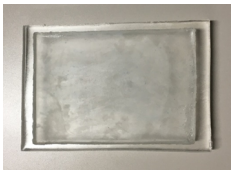

Fig. 1. The dummy skin

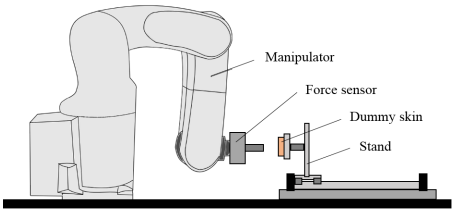

Fig. 2. The impact experimental apparatus

If the reaction time of the system is t_r, then the constraint of the state-space model in the brake part is that for $t = t_r$, moreover, the state variable is the same as the state variable in the runaway part. By solving this state-space model under the constraints, we can obtain the trajectories of the end-effector. We also define the stopping time, t_s, as the time when $\dot{x}_h(t_s) = 0$.

III. Impact experiment

A. Impact experiment using dummy skin

In this study, we assume contact between a dummy skin and a manipulator, which reproduces the characteristics of human skin. Therefore, to represent the dummy skin [23] in the aforementioned five-element Maxwell model, impact experiments were conducted to identify the parameters of the model. A manipulator with a $14\,\mathrm{mm}$ square impactor attached to an end-effector was used for the impact experiments. The stability forces were set at $5, 10, 15\,\mathrm{N}$, and the contact speed was set at $250\,\mathrm{mm/s}$. The experiments were repeated three times under different conditions.

B. Curve fitting

By defining the five-element Maxwell model, as shown in the Fig. 3, we obtain the following equation:

$$x = \begin{cases} vt & (0 \leq t < t_p) \\ vt_p & (t_p \leq t) \end{cases} \quad (13)$$

$$F = \begin{cases} k_1 vt + c_2 v[1 - \exp(-\frac{k_2}{c_2}t)] & \\ +c_3 v[1 - \exp(-\frac{k_3}{c_3}t)] & (0 \leq t < t_p) \\ k1vt_p + c_2 v[1 - \exp(-\frac{k_2}{c_2}t_p)] & \\ \exp[-\frac{k_2}{c_2}(t - t_p)] & \\ +c_3 v[1 - \exp(-\frac{k_3}{c_3}t_p)] & \\ \exp[-\frac{k_3}{c_3}(t - t_p)] & (t_p \leq t) \end{cases} \quad (14)$$

$$F_s = k_1 x(t_p) \quad (15)$$

where x is the displacement, v is the contact velocity, F is the contact force, F_s is the stable contact force, and t_p

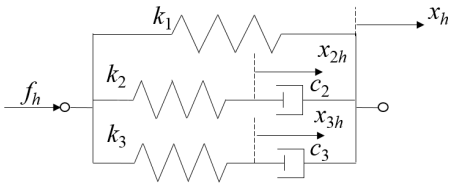

Fig. 3. 5-element Maxwell model

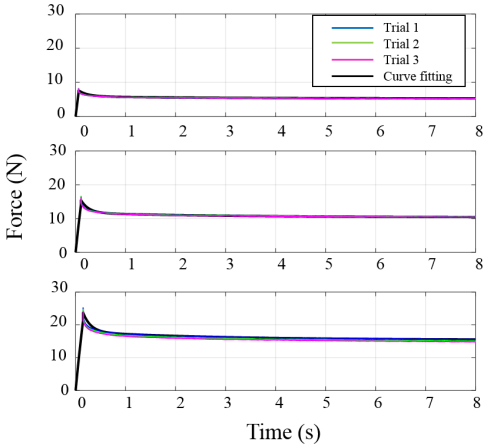

Fig. 4. Results of the impact experiments and curve fitting (from the top to bottom, stable force is 5 N, 10 N, 15 N)

is the peak value timing (or stop timing). Curve fitting was performed using these equations to optimize the viscoelastic parameters.

C. Result of curve fitting

The results of the curve fitting are presented in Fig. 4. The average value of the parameters obtained for each trial was used as the viscoelasticity parameter in the simulation. Table 1 shows the result of estimating the parameters of the 5-element Maxwell model for the dummy skin.

IV. Simulation of FSCMC

A. Condition of simulation

This section presents the simulations for evaluating the FSCMC. In this study, we focus on the CRANE-X7, a manipulator with three degrees of freedom by fixing 1,3,5 and 7 joints which are defined in Fig.5. We compare the combination of stopping only by braking without active joints and speed reduction via braking with active joints. The positional relationship between the manipulator and the dummy skin is shown in Fig. 6. It is assumed that the dummy skin is pressed against the workbench with a set initial velocity. The initial velocity is changed between $0\,mm/s$ and $100\,mm/s$. And the reaction time of the system is defined as $t_r = 50\,ms$. In this time of simulation, each normally operating joint rotates in the opposite direction to that where the robot moves to cause more hazardous situation.

B. Result of simulation

A part of the simulation results are shown in Fig. 7 through Fig. 9. In each graph, the horizontal axis is time

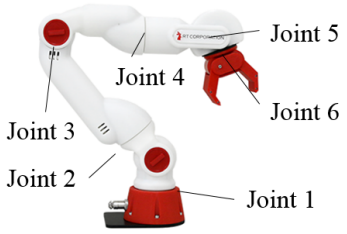

Fig. 5. CRANE-X7

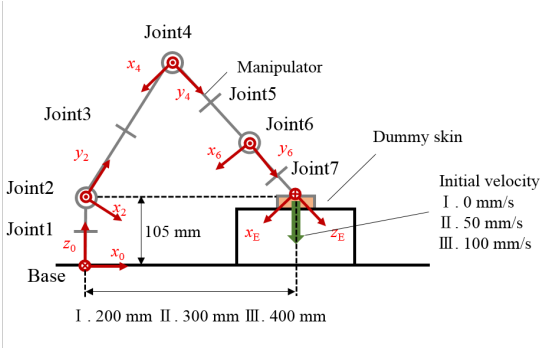

Fig. 6. The condition of the simulation

and the vertical axis is contact displacement of end-effector, and a legend is shown in the Fig. 7. The results show that the contact depth can be reduced by up to 1mm by using FSCMC.

C. Discussion

If there is a risk of robot-human contact, risk assessment shall take into account the severity of the risk and the probability of occurance of thebcontact. We have shown that the proposed FSCMC could reduce the severity of risk associated with injuries caused by such a contact. In the case where a contact is quasi-static (contact speed is nearly 0mm/s), the displacement curve appears convex during the runaway phase while the curve is drawn concave in the case where the contact speed is 100mm/s. With the proposed FSCMC incorporated, it is revealed to cause harmless events in the case of the quasi-static contact while harmful events can be anticipated in the situation of completely clamping a human hand. To what extent of speed can avoid any harmful event can become a novel criterion of HRC in contact tasks.

V. Conclusion

A fail-safe contact safety control (FSCMC) is proposed to reduce the contact risk of a human and a robot by making the most of healthy joints that can be controlled when a single failure occurs in a joint. The concept of fail-safe contact safety control is formulated and a method is proposed to generate torque to reduce contact risk using an active joint. Impact experiments were conducted to identify the viscoelastic parameters for a five-element Maxwell model of a dummy skin. Using simulations on CRANE-X7, the usefulness of FSCMC was investigated and it was shown that the displacement of end-effector can be reduced by up to $1\,mm$ in the case where the contact speed is 100mm/s. These

TABLE I

OPTIMIZED PARAMETERS OF THE 5-ELEMENT MAXWELL MODEL FOR THE DUMMY SKIN

Force (N)	k_1 (N/mm)	k_2 (N/mm)	k_3 (N/mm)	c_2 (N/(mm/s))	c_3 (N/(mm/s))
5	0.3652	0.1359	0.04154	0.0247	0.0915
10	0.3865	0.1944	0.04928	0.03037	0.1345
15	0.4143	0.2467	0.06681	0.03814	0.1748
Mean value	0.3869	0.1923	0.05254	0.03107	0.1336

results show that the method can possibly avoid serious accidents during a runaway caused by a single failure of a manipulator.

VI. ACKNOWLEDGE

This paper was financially supported by "Knowkedge Hub Aichi" research project: R7 and conducted through "Construction of Risk Assessment System for Service Robot Applications: Establishment of A V and V Testing Method." This paper is also financially supported by Kakenhi (Grant 20H02114: A novel strategy for safety control of a manipulator with a single fault detection capability to mitigate the severity of injury during a contact between the end effector of the manipulator and human skin under the worst case impact scenario.

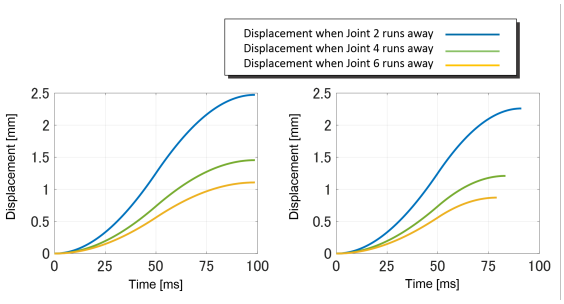

Fig. 7. Simulated result (Config. I, 0 mm/s,left=w/o AJ, right=w/ AJ)

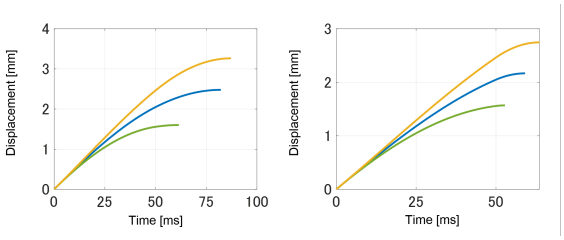

Fig. 8. Simulated result (Config. I, 50 mm/s,left=w/o AJ, right=w/ AJ)

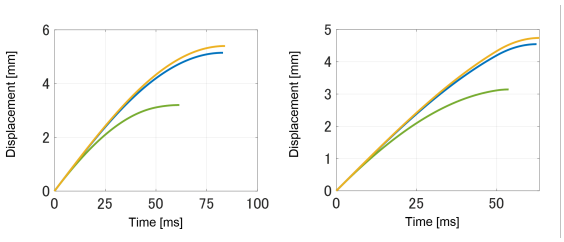

Fig. 9. Simulated result (Config. I, 100 mm/s,left=w/o AJ, right=w/ AJ)

REFERENCES

[1] "ISO10218–1,Robots for individual requirements –Safety requirements," 2010.

[2] B. Lacevic and P. Rocco, "Kinetostatic danger field-a novel safety assessment for human-robot interaction," in *2010 IEEE/RSJ International Conference on Intelligent Robots and Systems*. IEEE, 2010, pp. 2169–2174.

[3] B. Lacevic, P. Rocco, and A. M. Zanchettin, "Safety assessment and control of robotic manipulators using danger field," *IEEE Transactions on Robotics*, vol. 29, no. 5, pp. 1257–1270, 2013.

[4] S. Szabo, W. Shackleford, R. Norcross, and J. Marvel, *A testbed for evaluation of speed and separation monitoring in a human robot collaborative environment*. US Department of Commerce, National Institute of Standards and Technology, 2012.

[5] J. A. Marvel, "Performance metrics of speed and separation monitoring in shared workspaces," *IEEE Transactions on automation Science and Engineering*, vol. 10, no. 2, pp. 405–414, 2013.

[6] J. A. Marvel and R. Norcross, "Implementing speed and separation monitoring in collaborative robot workcells," *Robotics and computer-integrated manufacturing*, vol. 44, pp. 144–155, 2017.

[7] D. Kulić and E. Croft, "Pre-collision safety strategies for human-robot interaction," *Autonomous Robots*, vol. 22, no. 2, pp. 149–164, 2007.

[8] T. T. A. R. Sanderud, M. Niitsuma, "A likelihood analysis for a risk analysis for safe human robot collaboration," 2015.

[9] K. Sunada, Y. Yamada, T. Hattori, S. Okamoto, and S. Hara, "Extrapolation simulation for estimating human avoidability in human-robot coexistence systems," in *2012 IEEE RO-MAN: The 21st IEEE International Symposium on Robot and Human Interactive Communication*. IEEE, 2012, pp. 785–790.

[10] T. Hattori, Y. Yamada, S. Mori, S. Okamoto, and S. Hara, "Psychological experiments on avoidance action characteristics for estimating avoidability of harm to eyes from robots," in *2012 IEEE/RSJ International Conference on Intelligent Robots and Systems*. IEEE, 2012, pp. 5400–5405.

[11] K. Suita, Y. Yamada, N. Tsuchida, K. Imai, H. Ikeda, and N. Sugimoto, "A failure-to-safety" kyozon" system with simple contact detection and stop capabilities for safe human-autonomous robot coexistence," in *Proceedings of 1995 IEEE International Conference on Robotics and Automation*, vol. 3. IEEE, 1995, pp. 3089–3096.

[12] Y. Yamada, K. Suita, K. Imai, H. Ikeda, and N. Sugimoto, "A failure-to-safety robot system for human-robot coexistence," *Robotics and Autonomous systems*, vol. 18, no. 1-2, pp. 283–291, 1996.

[13] Y. Yamada, Y. Hirasawa, S. Huang, Y. Umetani, and K. Suita, "Human-robot contact in the safeguarding space," *IEEE/ASME transactions on mechatronics*, vol. 2, no. 4, pp. 230–236, 1997.

[14] T. Saito and H. Ikeda, "Measurement of human pain tolerance to mechanical stimulus of human-collaborative robots," *Specific Research Reports of the National Institute of Industrial Safety*, vol. 33, pp. 15–23, 2005.

[15] B. Povse, D. Koritnik, T. Bajd, and M. Munih, "Correlation between impact-energy density and pain intensity during robot-man collision," in *2010 3rd IEEE RAS & EMBS International Conference on Biomedical Robotics and Biomechatronics*. IEEE, 2010, pp. 179–183.

[16] T. Fujikawa, R. Sugiura, R. Nishikata, and T. Nishimoto, "Critical contact pressure and transferred energy for soft tissue injury by blunt impact in human-robot interaction," in *2017 17th International Conference on Control, Automation and Systems (ICCAS)*. IEEE, 2017, pp. 867–872.

[17] R. Sugiura, T. Fujikawa, R. Nishikata, and T. Nishimoto, "Soft tissue bruise injury by blunt impact in human-robot interaction-difference of tolerance between chest and extremities," in *2019 19th International*

Conference on Control, Automation and Systems (ICCAS). IEEE, 2019, pp. 792–797.

[18] "ISO10218-2, Robots and robotic devices–Safety requirements for industrial robots–Part 2: Robot systems and integration," 2011.

[19] D. Brambilla, L. M. Capisani, A. Ferrara, and P. Pisu, "Fault detection for robot manipulators via second-order sliding modes," *IEEE Transactions on Industrial Electronics*, vol. 55, no. 11, pp. 3954–3963, 2008.

[20] M. Van, P. Franciosa, and D. Ceglarek, "Fault diagnosis and fault-tolerant control of uncertain robot manipulators using high-order sliding mode," *Mathematical Problems in Engineering*, vol. 2016, 2016.

[21] L. M. Capisani, A. Ferrara, A. F. De Loza, and L. M. Fridman, "Manipulator fault diagnosis via higher order sliding-mode observers," *IEEE Transactions on industrial electronics*, vol. 59, no. 10, pp. 3979–3986, 2012.

[22] Y. Yamada, S. Takeda, T. Nishiyama, and S. Okamoto, "Potential runaway motion volume in task space for estimating the probability of occurrence of a human-robot collision," in *2018 IEEE International Conference on Intelligence and Safety for Robotics (ISR)*. IEEE, 2018, pp. 34–39.

[23] Y. Iki, Y. Yamada, Y. Akiyama, S. Okamoto, and J. Liu, "Designing a dummy skin by evaluating contacts between a human hand and a robot end tip."

[24] I. H. Nakazawa Nobuaki, Ikeura Ryojun, "Characteristics of human fingertips in the shearing direction."

[25] N. Yagasaki and H. Toyokawa, "The frequency of subcutaneous fat thickness of the japanese by sex and age."